CHAPTER II
THEORETICAL AND LITERATURE REVIEW

2.1 Activated arbon

Activated carbon is a carbonaceous material with a highly developed internal surface area and with a strong adsorptive capacity. Pyrolytic char can be converted into activated carbon by an appropriate physical activation process. Activated carbons produced from tire chars possess surface areas comparable with those of commercially available activated carbons. A pore system is developed using oxidizing agents such as carbon dioxide, air or steam, heated to 700–1000°C, creating new porous surfaces and with oxygenated functional groups (Helleur R. *et al.*, *2001*). Activated is a form of carbon that has been processed to make it extremely porous and thus to have a very large surface area available for adsorption or chemical reactions.

Figure 2.1 Activated carbon, as viewed by an electron microscope (*R. Helleur et al.*, *2001*).

Under an electron microscope, the high surface-area structures of activated carbon are shown. They showed various kinds of porosity. Moreover, they had flat surfaces of graphite-like material run parallel to each other and separated by only a few nanometers. Since adsorbing material can interact with many surfaces simultaneously. These micro pores good adsorption capacity.

2.2 Carbon Aerogel

Carbon aerogel is a highly solid porous material which extremely low densities, large open pore, and high specific surface areas. Moreover, its pore size can be controlled by changing starting material. The morphology of aerogel can be modified by using different synthesis parameters. This characteristic makes the aerogel particularly well adapted for various applications such as fuel cells, host material of catalysts, thermal insulators, and molecular sieves. The traditional process for organic aerogel preparation is typical via the sol–gel polymerization of an organic solution followed by supercritical drying of the obtained hydrogel to extract the solvent in the gel structure; and then they obtained organic aerogel is transformed into carbon aerogel via pyrolysis (*Pekala RW, 1989*). The total process of carbon aerogel preparation requires approximately 2 weeks. Recently, many attempts have been made to shorten the process, such as using alcohol-sol–gel polymerization and drying with supercritical acetone to avoid the solvent exchanging period (Qin G. and Guo S.1, *2001*). The organic and carbon aeorgel processing normally uses resorcinol (R) and formaldehyde (F) as the precursor. The RF aerogels consist of a highly crosslinked aromatic polymer. In order to obtain carbon aerogel, the RF gel is carbonized in an inert atmosphere. Basically, the crosslink density of organic gel is a key parameter that needs to be considered for aerogel applications. Highly crosslinked organic gel not only provides high structural stability in order to preserve its structure after solvent removal, but also introduces high char yield after pyrolysis to construct the carbon aerogel. In order to find a reactant to synthesize the

organic aerogel and transform it to carbon aerogel, these two characteristics of the synthesized gel need to be considered (*Lorjai et al., 2009*).

Carbon aerogels are obtained by pyrolysis of organic aerogels, which are mostly produced by the polycondensation reaction of resorcinol and formaldehyde in different solvents and using different catalysts (figure 2.2). They are generally supercritical dried prior to pyrolysis of the organic aerogels to preserve their pore texture (Faiŕen-Jiménez *et al.*, 2006).
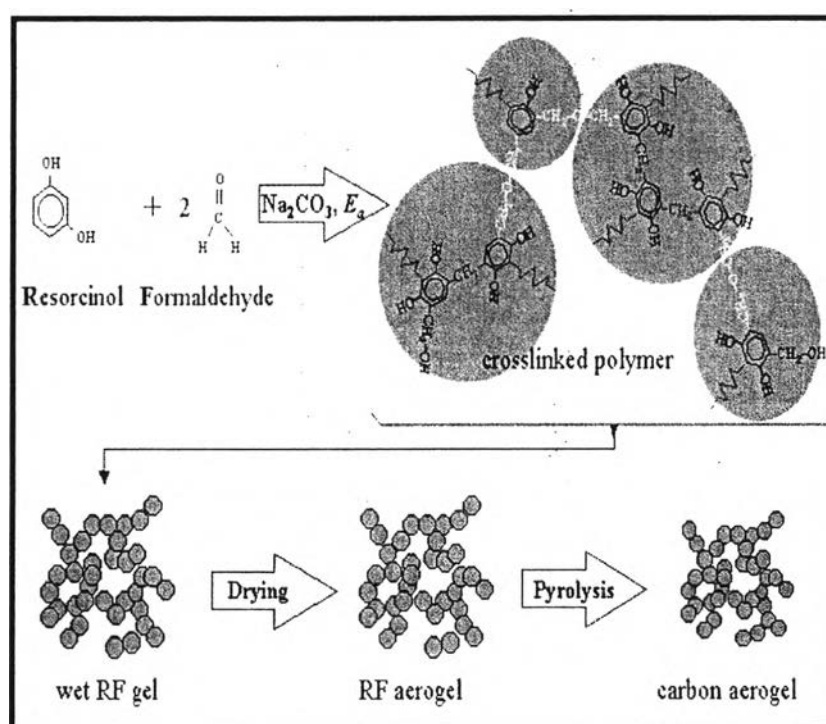

Figure 2.2 Schematic diagram of the reaction of resorcinol with formaldehyde (Berthon-Fabry and Achard, 2003).

The work done by Horikawa *et al.* in year 2003 showed that spherical resorcinol-formaldehyde(RF) aerogel particles were synthesized by emulsion polymerization of resorcinol with formaldehyde in a slightly basic aqueous solution, followed by supercritical drying with carbon dioxide. RF carbon aerogel particles were prepared by

carbonizing of the RF aerogel at high temperature nitrogen under a nitrogen atmosphere. By changing the viscosity of the RF sol added to the cyclohexane containing   a surface-active agent for preparation of the spherical RF hydrogels, RF aerogel particles with a truly spherical shape and controlled particle size were prepared. The spherical RF carbon aerogel particles had an average diameter of 20 μm, a BET surface area of about $800m^2/g$ and a uniform mesopores radius of 1.78 nm.

Chaisuwan et al. (2006) incorporated the maleimide functionality into the monofunctional benzoxazine resulting in increasing of char yield and glass-transition temperature without in increase the viscosity of the monomer.

Lorjai et al.(2009) prepared carbon aerogel from Bisphenal-A and aniline base polybenzoxazine(figure 2.3). They found that pore structure of carbon aerogel can be tailored by varying monomer concentration.
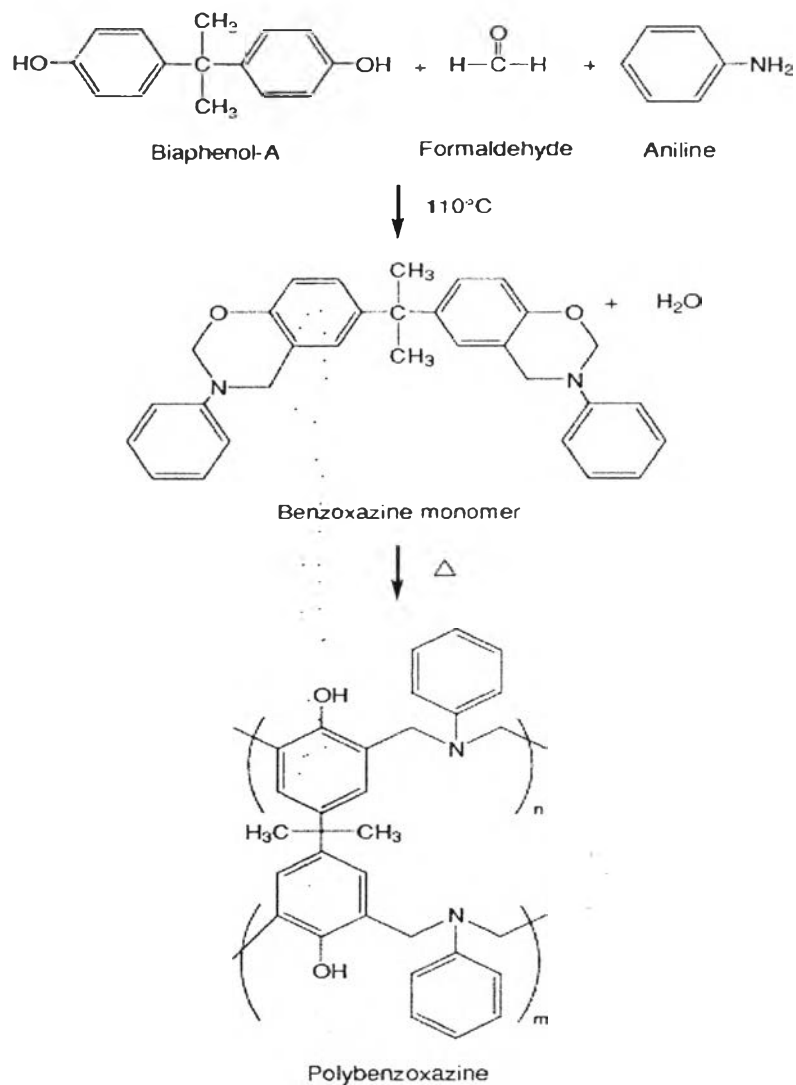
Figure 2.3 Schematic Precursors and the polybenzoxazine synthetic reaction.

Tamon H. *et al.* (1998) studied the mesoporous structure of organic and carbon aerogels by taking into account the synthesis conditions of the RF aquagels. They concluded that the mesoporous radius of the RF aerogel could be controlled in the range of 2.5-9.2 nm by changing the mole ratio of resorcinol to sodium carbonate used as a catalyst and the ratio of resorcinol to distilled water used as a diluent. Shrinkage also played a role in control of the mesopore redius. As the pyrolysis temperature increased,

the mesopore volume became small but the peak radius of pore distribution was maintained. It was also noticed that with an increase in the pyrolysis temperature, ethane adsorption became larger than ethylene adsorption on the aerogels. The carbon aerogels prepared by pyrolysis at 1000°C had the same ethane and ethylene adsorption characteristics as activated carbons did.

Mahingsupan N.(2010) studiedeffect of activation process on the pore structure of polybenzoxazine-derived carbon aerogel. By activating carbon aerogel at 900°C in CO_2 it was found that the activated carbon aerogel had a high surface area with large amount of micropores whereas the non-activated sample had lower surface area, but larger pore size are summarized in Table 2.1.

Table 2.1 surface areas, pore volume and pore diameter of carbon aerogels prepared from benzoxazine precursor

Parameter	CA	Heat-treated CA	Activated CA
BET surface area (m^2/g)	360	372	910
Total pore volume (cm^3/g)	0.24	0.25	0.54
Average pore size (nm)	2.69	2.65	2.40
Micropore volume (cm^3/g)	0.14	0.16	0.40
Mesopore volume (cm^3/g)	0.13	0.11	0.17
*Mesoporosity (%)	54.2	44.0	31.5
*Microporosity (%)	58.3	64.0	74.1

*Mesoporosity = (mesopore volume/total pore volume) × 100

*Microporosity = (micropore volume/total pore volume) × 100

2.3 Vegetable Oils

The use of vegetable oils, such as palm, soybean, sunflower, peanut and olive oils as alternative fuels for diesel engines dated back almost ten decades ago. Due to the rapid decline in crude oil reserves, the use of vegetable oils as diesel fuels is again promoted in many countries. Depending upon climate and soil conditions, different nations are looking into different vegetable oils for diesel fuels. For example, soy bean oil in the United States, rapeseed and sunflower oils in Europe, palm oil in Southeast Asia (mainly Malaysia and Indonesia), and coconut oil in the Philippines are being considered as substitutes for diesel fuels (Srivastava and Prasad, 2000). Vegetable oils are triglycerides which are esters of one glycerol with three long-chain acids (which can be different types), commonly called fatty acids. The major component of vegetable oils is triglycerides. Vegetable oils comprise 90 to 98% triglycerides and small amounts of monogylcerides and diglycerides. They contain free fatty acids (generally 1 to 5%) and traces of water (Srivastava and Prasad, 2000). The general formation of triglyceride is shown below.
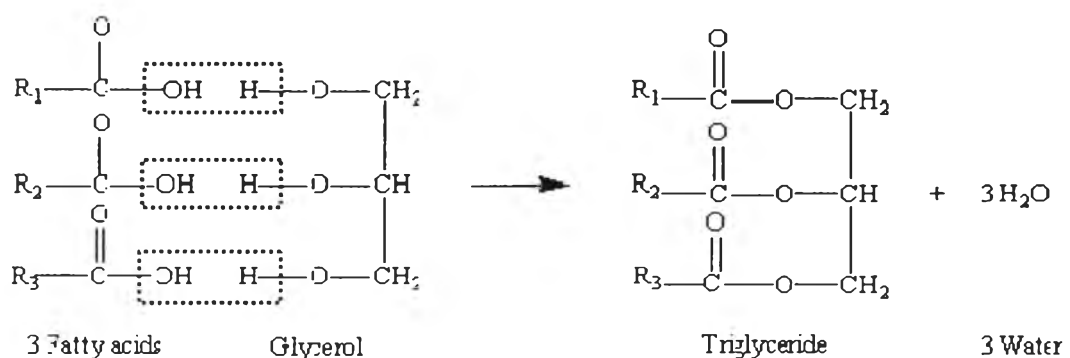
Figure 2.4 General formation of triglyceride (Swern, 1979).

From Figure 2.4, R_1, R_2 and R_3 represent a chain of carbon atoms with hydrogen atoms attached. The differences of R_1, R_2 and R_3 result in different types of fatty acids which glycerol will be combined. Different fatty acids have different carbon chain length and number of double bonds. This reason leads to make different characteristics of vegetable oil. The common fatty acids found in vegetable oils are stearic, palmitic, oleic, linoleic and linolenic. The name and chemical structure of common fatty acids are shown in Table 2.2. Fatty acid compositions in different types of vegetable oils are summarized in Table 2.2 and some properties of the vegetable oils are shown in Table 2.4.

Table 2.2 Chemical structure of common fatty acids (Srivastava and Prasad, 2000)

Fatty acid	Systematic name	Structure[a]	Formula
Lauric	Dodecanoic	12:0	$C_{12}H_{24}O_2$
Myristic	Tetradecanoic	14:0	$C_{14}H_{28}O_2$
Palmitic	Hexadecanoic	16:0	$C_{16}H_{32}O_2$
Stearic	Octadecanoic	18:0	$C_{18}H_{36}O_2$
Arachidic	Eicosanoic	20:0	$C_{20}H_{40}O_2$
Behenic	Docosanoic	22:0	$C_{22}H_{44}O_2$
Lignoceric	Tetracosanoic	24:0	$C_{24}H_{48}O_2$
Oleic	cis-9-Octadecenoic	18:1	$C_{18}H_{34}O_2$
Linoleic	cis-9,cis-12-Octadecadienoic	18:2	$C_{18}H_{32}O_2$
Linolenic	cis-9,cis-12,cis-15-Octadecatrienoic	18:3	$C_{18}H_{30}O_2$
Erucic	cis-13-Docosenoic	22:1	$C_{22}H_{42}O_2$

[a]xx:y indicates x carbons with y double bonds in fatty acid chain

Table 2.3 Fatty acid composition in different types of vegetable oils (Srivastava and Prasad, 2000)

Vegetable oil	Fatty acid composition, wt.%									
	14:0	16:0	18:0	20:0	22:0	24:0	18:1	22:1	18:2	18:3
Corn	0	12	2	tr	0	0	25	0	6	tr
Cottonseed	0	28	1	0	0	0	13	0	58	0
Crambe	0	2	1	2	1	1	19	59	9	7
Linseed	0	5	2	0	0	0	20	0	18	55
Peanut	0	11	2	1	2	1	48	0	32	1
Rapeseed	0	3	1	0	0	0	64	0	22	8
Safflower	0	9	2	0	0	0	12	0	78	0
H.O. Safflower	tr	5	2	tr	0	0	79	0	13	0
Sesame	0	13	4	0	0	0	53	0	30	0
Soya bean	0	12	3	0	0	0	23	0	55	6
Sunflower	0	6	3	0	0	0	17	0	74	0

[a]tr = traces.

Table 2.4 Properties of the vegetable oils (Marchetti *et al.*, 2007)
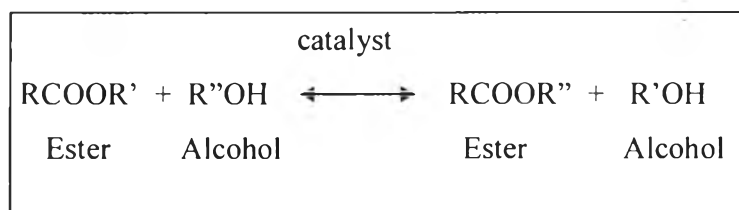
Vegetable oil	Kinematics viscosity (mm²/s)	Cetane number	Cloud point (°C)	Pour point (°C)	Flash point (°C)	Density (kg/l)	Lower heating value (MJ/kg)
Peanut	4.9	54	5	-	176	0.883	33.6
Soya bean	4.5	45	1	-7	178	0.885	33.5
Babassu	3.6	63	4	-	127	0.875	31.8
Palm	5.7	62	13	-	164	0.880	33.5
Sunflower	4.6	49	1	-	183	0.860	33.5
Tallow	-	-	12	9	96	-	-
Diesel	3.06	50	-	-16	76	0.855	43.8
20% biodiesel blend	3.2	51	-	-16	128	0.859	43.2

As shown in Table 2.4, the use of vegetable oils directly as diesel fuels leads to a number of problems. The injection, atomization and combustion characteristics of vegetable oils in diesel engines are significantly different from those of petroleum-based diesel fuels. Due to the high viscosity of vegetable oils, the injection process is interfered and leads to poor fuel atomization. Moreover, the high flash point attributes to its low volatility characteristics. This leads to more deposit formation and carbonization. In addition, the combination of high viscosity and low volatility of vegetable oils causes poor cold engine start up and ignition delay. In the long-term operation, vegetable oils normally develop gumming, injector coking and ring sticking (Srivastava and Prasad, 2000). Therefore, considerable efforts must be made to develop vegetable oil derivatives that close to the properties and performance of the petroleum-based diesel fuels.

2.4 Derivatives of Triglycerides as Biodiesel

As previous described, there are many problems associated with the use of vegetable oils directly as fuels for diesel engine since they have high viscosity, low volatility and some polyunsaturated fatty acids. To overcome these problems, the oil requires slight chemical modifications which mainly are pyrolysis, dilution, microemulsification, and transesterification. Among these processes, transesterification is the most commonly used method to produce the cleaner and environmentally safe biodiesel from vegetable oils.

Transesterification or alcoholysis is the reaction of fat or oil with an alcohol to form esters and glycerol. A catalyst (a strong acid or base) is usually used to improve the reaction rate and yield. This process has been widely used to reduce the high viscosity of triglycerides (Meher et al., 2006). The transesterification reaction is represented by a general equation, as shown in Figure 2.5.

$$
\begin{array}{c}
\text{catalyst} \\
\text{RCOOR'} + \text{R''OH} \xrightleftharpoons{} \text{RCOOR''} + \text{R'OH} \\
\text{Ester} \qquad \text{Alcohol} \qquad\qquad \text{Ester} \qquad \text{Alcohol}
\end{array}
$$

Figure 2.5 General equation of transesterification reaction (Srivastava and Prasad, 2000).

Generally, the alcohols used in the transesterification process are methanol, ethanol, propanol, butanol, and amyl alcohol. Methanol and ethanol are the most frequently used, especially methanol because of its low cost and its physical and chemical advantages (polar and shortest chain alcohol). It can quickly react with triglycerides and NaOH catalyst is easily to dissolve in it (Fangrui and Hanna, 1999). If methanol is used in this process, it is called methanolysis, as presented in Figure 2.6.
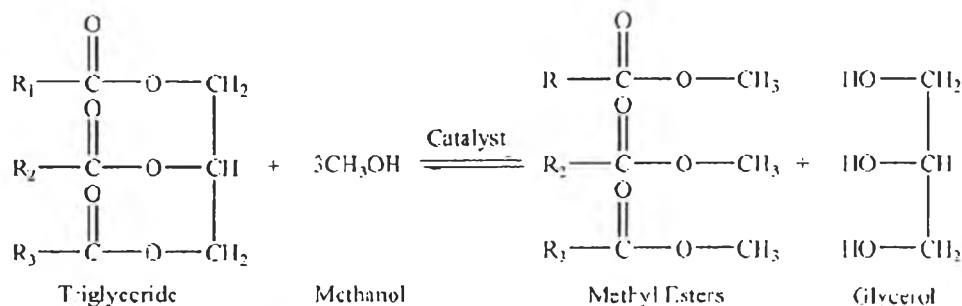
Figure 2.6 Methanolysis of triglyceride (Srivastava and Prasad, 2000).

Due to the transesterification is one of the reversible reactions and proceeds essentially by mixing the reactants; therefore, the excess methanol is required to shift the equilibrium to the products side. To complete a transesterification stoichiometrically, a 3:1 molar ratio of methanol to triglycerides is needed. In practice, the ratio needs to be higher to drive the equilibrium to a maximum methyl ester yield. The methyl ester products (known as biodiesel) are attractive as alternative diesel fuels.

2.5 Biodiesel

Biodiesel refers to a non-petroleum-based diesel fuel consisting of short chain alkyl (methyl or ethyl) esters, made by transesterification of vegetable oil or animal fat (tallow), which can be used (alone, or blended with conventional petro diesel) in unmodified diesel-engine vehicles. Biodiesel is distinguished from the straight vegetable oil (SVO) (sometimes referred to as "waste vegetable oil", "WVO", "used vegetable oil", "UVO", "pure plant oil", "PPO") used (alone, or blended) as fuels in some converted diesel vehicles. "Bio diesel" is standardized as mono-alkyl ester and other kinds of diesel-grade fuels of biological origin are not included.

Biodiesel is a biodegradable and non-toxic alternative fuel produced from new or used vegetable oil that is produced from renewable resources. It can be used in any Diesel engine without modification. Pure biodiesel has the highest BTU content of any

alternative fuel. It also has the highest energy balance of any fuel. For every unit of fossil energy needed to produce biodiesel, more than 3 units of energy are gained. As for gasoline and diesel, every one unit put in yields only about one half units. Because biodiesel is made from plant oil or animal fat and not from 40,000,000 year old organic matter, it is renewable. Moreover, the carbon dioxide taken up by plants during photosynthesis helps to mitigate the carbon dioxide emitted from using biodiesel so there is no net carbon introduced to the atmosphere. Compared to diesel fuel, biodiesel emissions are substantially better for the environment and, in turn, better for the health of the environment's inhabitants. Specifically, the emissions of particulate matter, carbon monoxide and total unburned hydrocarbons from biodiesel are each much less than those from petroleum diesel.

The properties of biodiesel and petroleum-based diesel fuels are compared and shown in Table 2.5. From this table, it shows that biodiesel produced from various vegetable oils have viscosities close to those of petroleum-based diesel fuels. Their heating values are a little lower, but they have high cetane numbers and flash points. Since the characteristics of biodiesel are generally similar to those of petroleum-based diesel fuels; therefore, biodiesel is a strong candidate to replace petroleum-based diesel fuels.

Table 2.5 Comparison between properties of biodiesel and petroleum-based diesel fuels (Fukuda et al., 2001).

Vegetable oil methyl ester	Kinematic viscosity (mm2/s)	Cetane number	Lower heating value (MJ/l)	Cloud point (°C)	Flash point (°C)	Density (g/l)	Sulfur (wt%)
Peanut	4.9 (37.8°C)	54	33.6	5	176	0.883	-
Soybean	4.5 (37.8°C)	45	33.5	1	178	0.885	-
Babassu	3.6 (37.8°C)	63	31.8	4	127	0.879	-
Palm	5.7 (37.8°C)	62	33.5	13	164	0.880	-
Sunflower	4.6 (37.8°C)	49	33.5	1	183	0.860	-
Rapeseed	4.2 (40°C)	51-59.7	32.8	-	-	0.882	-
Used rapeseed	9.48 (30°C)	53	36.7	-	192	0.895	0.002
Used corn oil	6.23 (370°C)	63.9	42.3	-	166	0.884	0.0013
Diesel fuel	12-3.5 (40°C)	51	35.5	-	-	0.830-0.840	-
JIS-2D (gas oil)	2.8 (30°C)	58	42.7	-	59	0.833	0.05

There are many advantages for using biodiesel. For example, it is renewable resource, biodegradable, nontoxic and essentially free of sculpture and aromatics, makes it has low emissions of SO_x, CO, NO_x, unburn hydrocarbon and particulate matter as compared to conventional diesel fuel (Karmee et al., 2005). It can be used without engine modification, generates good engine performance and improves combustion because of its oxygen content. Furthermore, it offers good lubrication properties and ability to be blended in any proportion with regular petroleum-based diesel fuel.

However, some biodiesel properties such as oxidative stability and cold flow properties depend on natural characteristic of starting vegetable oil. The oxidative stability has been found to be concerned when the biodiesel is stored over an extended period of time due to the presence of significant amount of unsaturated fatty acid methyl esters (FAMEs). The storage problems can be caused by storage conditions like exposure to air, light, as well as temperature. This fuel instability leads to the sediment and gum formation and fuel darkening. Moreover, the oxidation process during storage produces hydroperoxides, aldehydes, ketones, and acids (Nikolaou *et al.,* 2009), which causes operational problems like fuel filter plugging, injector fouling, and deposit formation in engine combustion chamber (Yamane *et al.,* 2007). Biodiesel produced from vegetable oil which contains high amount of saturated fatty acid has higher oxidative stability. However, the higher amount of saturated fatty acid gives the lower cold flow property (Sonthisawate *et al.,* 2008). The amount of unsaturation in fatty acid can be determined by iodine value, which is the mass of iodine in grams that is consumed by 100 grams of a chemical substance (www.wikipedia.org). Generally, vegetable oils usually contain free fatty acids, phospholipids, sterols, water, odorants and other impurities. Because of these, the oil cannot be used as fuel directly (Meher et al., 2006). To overcome these problems, the oil requires slight chemical modifications which mainly are pyrolysis, dilution, microemulsification and transesterification as previously described. Among these, transesterification is the most commonly used method to produce the cleaner and environmentally safe biodiesel from vegetable oils. The details on transesterification of vegetable oils are described below.

2.6 Transesterification of Vegetable Oils

Currently, transesterification of vegetable oils is the most commonly used method for biodiesel production. In this process, a triglyceride which is the main component in vegetable oils reacts with an alcohol, producing a mixture of fatty acids alkyl esters which are well known in name of biodiesel and co-product glycerol. The stoichiometric reaction requires 1 molecule of triglyceride and 3 molecules of alcohol. The overall transesterification reaction is shown in Figure 2.7. However, an excess of the alcohol is used to increase the yields of the alkyl esters and to allow its phase separation from the formed glycerol (Schuchardta et al., 1998).
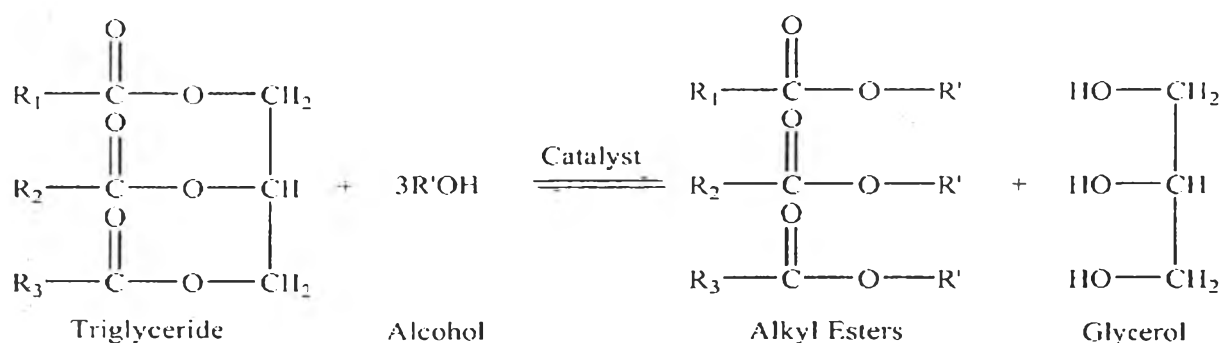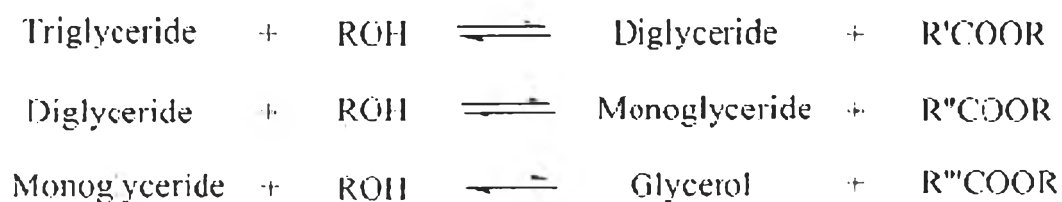

Figure 2.7 Overall transesterification reaction (Schuchardta et al., 1998).

Many types of alcohol can be used in the transesterification reaction such as methanol, ethanol, propanol, butanol and amyl alcohol. Methanol and ethanol are the most frequently used, especially methanol because of its lowest cost when compare to other alcohols and its physical and chemical advantages (polar and shortest chain alcohol). It can quickly react with triglyceride resulting in higher conversion of triglyceride to alkyl esters (Fangrui and Hanna, 1999).

The transesterification reaction consists of sequence of three consecutive reversible reactions as shown in Figure 2.8. The first step, triglyceride is converted to diglyceride. The second, diglyceride is converted to monoglyceride and finally,

monoglyceride is converted to glycerol. In each step, one molecule of methyl ester is liberated (Srivastava and Prasad, 2000).

Triglyceride + ROH $\rightleftharpoons$ Diglyceride + R'COOR

Diglyceride + ROH $\rightleftharpoons$ Monoglyceride + R''COOR

Monogyceride + ROH $\rightleftharpoons$ Glycerol + R'''COOR

Figure 2.8 The step of transesterification reaction of vegetable oil (Meher *et al.*, 2006).

A review done by Srivastava and Prasad (2000) summarized the important variables that influence transesterification and ester conversion. These variables are reaction temperature, alcohol to oil ratio, catalyst type, catalyst concentration, mixing intensity and purity of reactants. The maximum yield of alkyl esters occurs at temperature close to boiling point of the used alcohol at a molar ratio of alcohol to oil equal 6:1. They also pointed out that the basic homogeneous catalyst like sodium alkoxide is the most effective for transesterification. However, the presence of free fatty acids and water can cause some side reactions thereby affecting the ester conversion.

Basically, transesterification of vegetable oil can also proceed in the absence of a catalyst but reaction temperature and pressure should high enough. Diasakou *et al.* (1998) reported that the ester conversion was over 85% after 10 hours of reaction for non-catalytic methanolysis of soybean oil at 235°C and 62 bars. However, non-catalytic transesterification hardly makes sense from an economic point of view due to the high reaction temperature and pressure requirement and long reaction time is required. Thus, to achieve satisfactory ester yield under mild condition, biodiesel production is generally conducted in the presence of catalyst.

2.7 Partial Hydrogenation

Hydrogenation is the chemical reaction that results from the addition of hydrogen (H_2). The process is usually employed to reduce or saturate organic compounds. This process typically constitutes the addition of pairs of hydrogen atoms to a molecule, since non-catalytic hydrogenation takes place only at very high temperature and pressure. So, catalysts are required to reduce the operating temperature and pressure for this reaction to be useable.

Partial hydrogenation is a process that hydrogen atoms are added to partially saturate double bond in the fatty acid methyl esters (FAMEs) structure. This process requires low pressure and temperature at about 1–5 bar and 80–120°C. The main objective of partial hydrogenation is to saturate the polyunsaturated FAMEs (C18:3 and C18:2) to the monounsaturated one (C18:1), in order to obtain biodiesel product with relatively high oxidative stability and good cold flow properties (Yoshimura, 2009). The schematic of partial hydrogenation of polyunsaturated FAME is shown in Figure 2.9
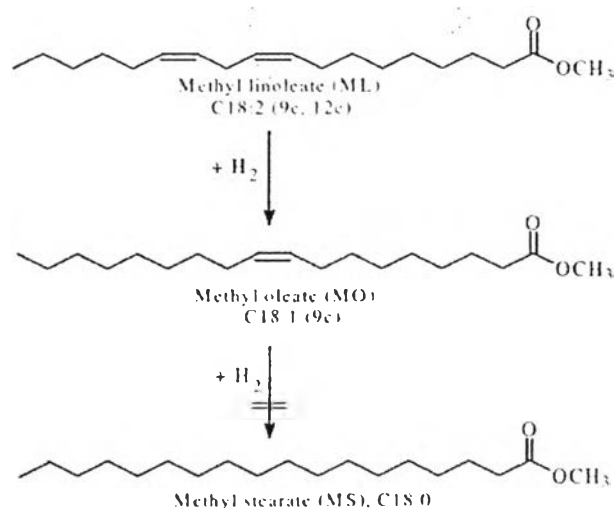
Figure 2.9 Partial hydrogenation of polyunsaturated FAME (Nicolaou *et al.*, 2009)

From previous work of Kapilla and co-workers showed that the properties of hydrogenated FAME strongly depend on the hydrogenation time. The total percentage of saturated fatty acid (SFA) increased from 29.3% to 76.2% after 2 h of hydrogenation. So, they can conclude that hydrogenation is a good method to increase oxidative stability as well as higher cetane number, which are two key parameter for biodiesel. However, the poorer cold flow properties of hydrogenated FAME make it unsuitable for cold weather condition.

In addition, Nicolous and co-workers studies the partial hydrogenations of polyunsaturated FAMEs selectively to monounsaturated compounds using active rhodium sulfonated phosphate (Rh/STPP) complexes. They found that partial hydrogenation substantially increase the oxidative stabilities and greatly improve the ageing/storage properties of biodiesel product and is not influence to cold flow property.

In 2006 Snare and co-worker studied and the result showed that Pd supported on carbon is the best partial hydrogenation catalyst in term of high activity and high selectivity compare to other metal catalyst on different supports.

Furthermore, the previous work done by Tamai et al. in year 2009 showed that Pd particles supported mesoporous activated carbons were prepared by immersing mesoporous activated carbons in a dispersion of Pd particles and their catalytic activities for the hydrogenation of methyl linoleate were investigated. As a result, they found that Pd particles were mainly supported on mesopores. Pd supported mesoporous activated carbons exhibited high catalytic activities, compared with Pd supported microporous activated carbon. It is indicated that Pd particles supported on mesopores play an important role in the catalytic activity.

2.8 Diesel Fuel

Diesel or Diesel fuel in general is any fuel used in diesel engines. The most common is a specific fractional distillate of petroleum fuel oil, but alternatives that are not derived from petroleum, such as biodiesel, biomass to liquid (BTL) or gas to liquid (GTL) diesel, are increasingly being developed and adopted. To distinguish these types, petroleum-derived diesel is increasingly called petrodiesel Ultra-low sulfur diesel (ULSD) is a term used to describe a standard for defining diesel fuel with substantially lowered sulfur contents.

Because of diesel engine have a difference size, so diesel fule must have suitable properties for each diesel engine

2.8.1 Ignition Quality (Cetane Number)

The performance of diesel engines is critically dependent upon the ignition quality of the fuel. The diesel engine relies on the high pressures and temperatures generated during the compression stroke to bring about auto-ignition of the air-fuel mixture. Auto-ignition is defined as the condition when the air-fuel mixture spontaneously ignites without an external source of ignition, such as flame or spark. The tendency of the diesel fuel to ignite under these conditions is known as its ignition quality, which is conveniently expressed in terms of the cetane number. The higher cetane number, the better the ignition quality. Higher cetane number shortens the ignition delay period, which translates to smoother combustion and thereby optimising the power generated. Cetane number also influences cold start performance, white smoke, engine noise, and emission.

2.8.2 Sulphur Content

Sulphur content of On-Road Diesel Fuel cannot exceed 22 mg/kg after September 1, 2006 and 15 mg/kg after October 15, 2006. These ultra-low sulphur levels are mandated by Federal legislation and required for all 2007 model year vehicles that will be equipped with advanced emission control systems utilizing diesel particulate filters (DPFs) in exhaust systems. High sulphur fuel will be potentially harmful because it will result in premature filter plugging with sulphates.

2.8.3 Lubricity

Lubricity is the ability to reduce friction between two surfaces in relative motion. It is a measure of fuel's effectiveness as a lubricant. Diesel fuel also functions as lubricant in fuel injection equipment such as rotary or distributor- type injection pumps, and injectors. The severe hydro treatment process involved to lower the sulphur content of the diesel fuel to where it is now tends to reduce its natural lubricating properties. Lubricity additives are used to enhance the lubricating property of this severely hydro treated diesel fuel. Industry standards require diesel fuel to provide acceptable performance in accordance with prescribed test methods. Increased wear in the fuel injection system will cause insufficient fuel delivery and will lead to poor engine driveability. In the long term and in extreme cases fuel pumps and injectors will seize and breakdown.

2.8.4 Cloud Point

Cloud point is the temperature at which wax crystals begin to form in the fuel. The cloud point temperature of the diesel fuel indicates how well it performs at low temperatures. This property is important because wax crystals can block fuel filters, thus starving the engine of fuel. The industry standard for supplying Diesel Fuel is to ensure the cloud point does not exceed a prescribed temperature for a given half-month period.

2.8.5 Flash Point

Flash point is the lowest temperature at which the diesel fuel will start to emit vapor that can be ignited by an external source. Flash point has no direct influence on engine performance, but it is important for safe storage, handling, and transport of diesel fuel. A low flash point fuel can be a fire hazard. In addition, low flash point may provide an indication of contamination with more volatile fuels- such as gasoline.

2.8.6 Viscosity

Viscosity is a measure of a liquid's resistance to flow under pressure and is dependent upon temperature. At higher temperature, the viscosity of the fuel decreases and at lower temperature its viscosity increases. Viscosity of diesel fuel influences engine performance in two ways: injection pump and injector performance, and injected fuel spray pattern and atomization. A very low viscosity fuel can cause internal leakages in the injection pump causing low pressure build up resulting to fuel starvation in the combustion chamber of the engine. This could also lead to undesirable spray pattern that promotes incomplete combustion. Fuel starvation and incomplete combustion will both contribute to reduced power and excessive emission. A very low viscosity fuel also causes excessive wear in the injection system and poor hot re-start.

On the other hand, a very high viscosity fuel will cause poor atomization during injection. As a result, the fuel is not evenly distributed in the combustion chamber to mix well with the air - a requisite for good combustion.

2.8.7 Volatility (Distillation)

The distillation characteristics of a diesel fuel impart an important influence on diesel engine performance. Volatility of the diesel fuel tends to affect power output and fuel economy. A less volatile fuel tends to reduce power output and fuel economy due to poor atomization. A diesel fuel with too high volatility tends to promote vapor lock in the fuel system and unfavorable spray penetration from the injector thereby reducing power output and fuel economy. Distillation characteristics of diesel fuel also influence cold start exhaust smoke and odors.

2.8.8 Oxidation Stability

One important problem associated with renewable fuel derived from vegetable oil and animal fats (i.e., biodiesel) is poor oxidative stability. This is especially true for soy-based biodiesel which has significantly higher levels of polyunsaturation. Interestingly, it has been reported that the oxidative stability problem is more pronounced in 20% blended biodiesel (B-20) than in neat soy-based biodiesel (B-100), presumably due to the fact that ultra-low sulfur diesel (ULSD) is a much poorer solvent as compared to B-100. Another factor which may contribute to the oxidative instability is the presence of metal ions and additives in ULSD. This paper will examine three fundamental aspects: 1. The oxidative stability of individual fatty acid esters and soy-based biodiesel when blended with ULSD; 2. The effectiveness of synthetic and natural antioxidants as a function of concentration, storage time and conditions, in B-20; and 3. the catalytic effects of transition metal ions on the oxidative degradation of biodiesel and biodiesel blends. The oxidative stability will be evaluated by measuring the acid number, peroxide value, kinematic viscosity and Rancimat induction period. Based on the findings, the possible mechanisms leading to the oxidative degradation in B-20 will be discussed. Various approaches to minimize oxidative stability problems in B-20 will be examined.

2.9 Titanium (IV) Oxide

Titanium (IV) oxide is generally known as titanium dioxide or titania, appearing in white solid. Its chemical formula is TiO_2. Due to its brightness and high refractive index (n=2.7), titania is extensively used as a white pigment, providing whiteness and opacity to products, such as paints, plastics, papers, inks, cosmetics and toothpastes. It is also used in almost every sunscreen product due to its high ultraviolet light absorptivity. Fujishima *et al.* (1972) reported novel potential of titanium dioxide as photocatalyst. Recently, Kasuga (2005) informed utilizing modified titania nanotube in bone regeneration material and proton conduction electrolytic film.

2.9.1 Polymorphs

The general occurrence of titanium (IV) oxide in nature is well-known in three forms, viz. rutile, anatase and brookite. The polymorphs of titania reported to date include rutile, anatase, brookite, TiO_2-B (bronze), TiO_2-R (ramsdellite), TiO_2-H (hollandite), TiO_2-II (columbite), and TiO_2-III (baddeleyite). Details of this distinctive polymorph are listed in table 2.1 (Yang *et al.*, 2009).

Table 2.6 structural parameters of TiO_2 polymorphs

Structure	Space group	Density $(g\ cm^{-3})$	Unit cell (Å)
Rutile	P4$_2$/mnm	4.13	a = 4.59, c = 2.96
Anatase	I4$_1$/amd	3.79	a = 3.79, c = 9.51
Brookite	Pbca	3.99	a=9.17, b = 5.46, c=5.14
TiO_2 (B)	C2/m	3.64	a = 12.17, b = 3.74, c = 6.51, β = 107.29°
TiO_2 –II	Pbcn	4.33	a = 4.52, b = 5.5, c = 4.94
TiO_2 (H)	I4/m	3.46	a = 10.18, c = 2.97
TiO_2 – III	P2$_1$/c	C	a = 4.64, b = 4.76, c = 4.81, β = 99.2°
TiO_2 (R)	Pbnm	3.87	a = 4.9, b = 9.46, c = 2.96

Crystalline structure of titania is simply represented as octahedron which titanium atom surrounded by oxygen atom on the edge. Each polymorph of titania has its own arrangement of the octahedrons (Bokhimi*et al.*, 2001). Below, the crystalline structures of rutile and anatase are presented.
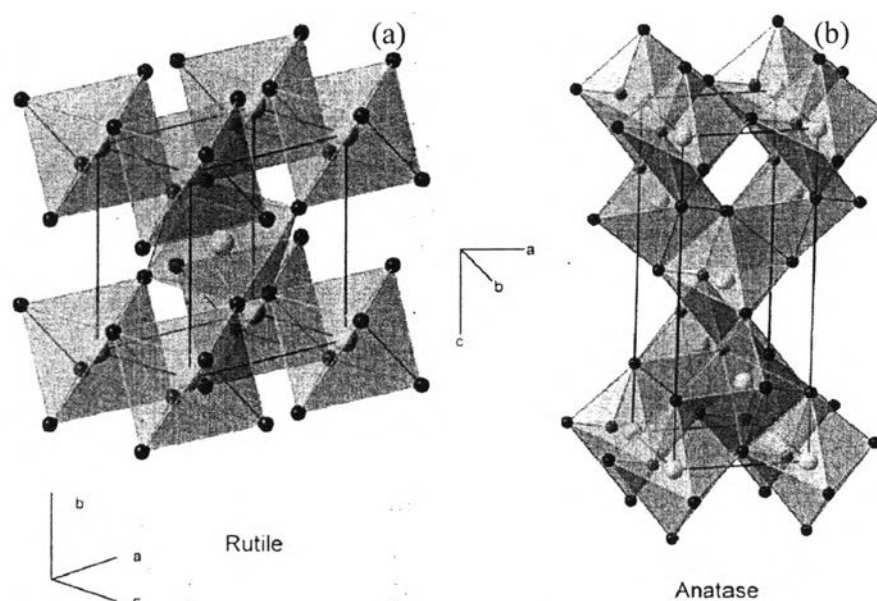

Figure 2.10 Crystalline structures of rutile (a) and anatase (b) (Yang *et al.*, 2009).

2.10 Semiconductor

A semiconductor is a material with an electrical conductivity that is intermediate between that of an insulator and a conductor. Like other solids, semiconductor materials have electronic band structure determined by the crystal properties of the material. A semiconductor used as photocatalyst should be an oxide or sulfide of metals, such as TiO_2, CdS, and ZnO. The actual energy distribution among electrons is described by the Fermi level and temperature of the electrons. At absolute zero temperature, all of the electrons have energy below the Fermi energy, but at non-zero temperature, the energy levels are randomized, and some electrons have energy above the Fermi level.

Among the bands filled with electrons, the one with the highest energy level is referred to as the valence band, and the band outside of this is referred to as the conduction band. The energy width of the forbidden band between the valence band and the conduction band is referred to as the band gap. The overall structure of band gap energy is shown in Figure 2.11.
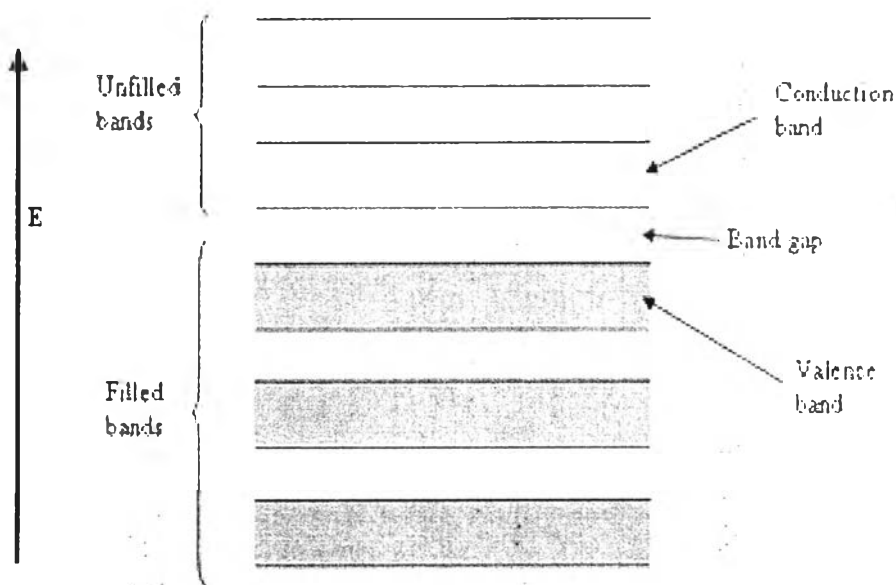
Figure 2.11 The structure of band gap energy.

The band gap can be considered as a wall that electrons must jump over in order to become free. The amount of energy required to jump over the wall is referred to as the band gap energy (E_g, eV). Only electrons that jump over the wall and enter the conduction band (CB, which are referred to as conduction band electrons) can move around freely. When light is illuminated at appropriate wavelengths with energy equal or more than band gap energy, valence band (VB) electrons can move up to the conduction band (CB). At the same time, as many positive holes as the number of electrons that have jumped to the conduction band (CB) are created. The valence band (VB), conduction band (CB),

band gap, and band gap wavelength of some common semiconductors are shown in Table 2.7.

Table 2.7 The band gap positions of some common semiconductor photocatalysts (Robertson, 1996; Vali, 2007; and Moreira *et al.*, 2009)

Semiconductor	Valence band (eV)	Conduction band (eV)	Band gap (eV)	Band gap wavelength (nm)
TiO_2	+3.1	-0.1	3.2	387
SnO_2	+4.1	+0.3	3.8	326
$SrTiO_3$	+3.1	-0.1	3.2	387
$SrZrO_3$	+4.3	-1.3	5.6	221
ZnO	+3.0	-0.2	3.2	387
ZnS	+1.4	-2.3	3.7	335
WO_3	+3.0	+0.2	2.8	443
CdS	+2.1	-0.4	2.5	496
CdSe	+1.6	-0.1	1.7	729
GaAs	+1.0	-0.4	1.4	886
GaP	+1.3	-1.0	2.3	539

2.11 Photocatalysts

Powders with semiconductor characteristics have been widely employed in photocatalytic systems because they are capable of generating charge carriers by absorbing photon energies. The separation effectiveness of the photo-induced charge carriers is an important factor in determining the photocatalytic activity of the powders. One promising photocatalyst is perovskite-related material. Perovskite-related materials are represented by the general formula of ABO_3 (A = rare earth and alkali element with or

without its partial substitution by alkaline earth element, and B = transition element, such as Co, Mn, Ti, Ta, Ni, Fe, etc., with or without its partial substitution)(Hu *et al.*, 2007).

Strontium titanate ($SrTiO_3$) is a well-known cubic-perovskite paraelectric oxide with a large dielectric constant, which has attracted a great deal of attention due to its excellent dielectric, photoelectric, optical, and catalytic properties. $SrTiO_3$ is also considered to be useful for photocatalytic decomposition of water in place of conventional photocatalysts, such as TiO_2, because its CB level provides a higher photopotential than TiO_2 and facilitates hydrogen formation (Subramanian *et al.*, 2006). However, pure $SrTiO_3$ without cocatalysts showed very low photocatalytic activity. Therefore, the modification of $SrTiO_3$ is necessary to obtain active catalysts for H_2 generation from pure water. For example, Ag, Cr, Pt, Rh, Pd, and Ta have been incorporated into $SrTiO_3$. The photocatalytic activity enhancement by Ag doping on $SrTiO_3$ was reported by Subramanian *et al.* (2006). $SrTiO_3$ doped with Cr^{3+} led to an introduction of isolated energy levels within its band gap, so photon can be absorbed at two levels, the band gap and the sub-band gap, where the latter led to light absorption in the visible region (Ashokkumar, 1998).

Puangpetch *et al.* (2008) investigated the synthesis and photocatalytic activity in methyl orange degradation of mesoporous-assembled $SrTiO_3$ nanocrystals prepared by sol-gel method with the aid of structure-directing surfactant. The results showed that the $SrTiO_3$ nanocrystals were successfully synthesized by using strontium nitrate ($Sr(NO_3)_2$) and tetraisopropyl orthotitanate (TIPT) as precursors. Anhydrous ethanol (EtOH), ethylene glycol (EG), or EtOH/EG was selected as a solvent, while laurylamine hydrochloride (LAHC), cetyltrimethylammonium bromide (CTAB), or cetyltrimethylammoniumchloride (CTAC) was used as a structure-directing surfactant. The effects of the photodegradation of methyl orange by the $SrTiO_3$, such as crystallinity, specific surface area, and pore characteristic, were investigated. The mesoporous-assembled structure with a high pore uniformity of $SrTiO_3$ plays the most important role affecting the photocatalytic activity of the $SrTiO_3$ photocatalyst. The $SrTiO_3$ with the mesoporous-assembled structure and narrow pore size distribution synthesized at a

calcination temperature of 700°C, a heating rate of 1°C min^{-1}, a LAHC-to-TIPT molar ratio of 0.25:1, and using an EtOH solvent provided the highest photocatalytic degradation activity, which was much higher than that of the non-mesoporous-structured commercial $SrTiO_3$.

Zielińska et al. (2008) investigated the photocatalytic efficiency of alkaline earth (Ca, Sr, Ba) titanate-based compounds for hydrogen generation. Their results showed that the addition of organic donors (such as formic acid, acetic acid, methanol, 2-propanol, and formaldehyde) enhanced the efficiency of the studied process. The systematic study has shown that the most efficient organic donor in regards to its hydrogen generation efficiency was formic acid. Of the catalysts explored, the highest photocatalytic activity was obtained by using $SrTiO_3:TiO_2$ composite.

Strontium zirconate ($SrZrO_3$) also belongs to the perovskite family and has an orthorhombic structure at room temperature with space group *Pbnm*. However, more recent studies on high-temperature investigation have shown that $SrZrO_3$ has the following sequence of phase transitions. First, orthorhombic (*Pnma*) was transformed to orthorhombic (*Cmcm*) at 973 K, then to tetragonal (*I4/mcm*) at 1,103 K, and finally the structure was found to be the ideal cubic perovskite (*Pm3m*) at 1,400 K (Feng et al., 2001). This compound has a high melting temperature of about 2,923 K, so it is cubic in a wide range of temperature where most of its useful applications take place. Perovskite oxides are important materials for various functional devices. $SrZrO_3$-based perovskite oxides have been studied for their high-temperature protonic conductivity, which makes them potential candidates for electrolytes in some novel electrochemical devices, such as solid oxide fuel cells and hydrogen sensors. Besides, $SrZrO_3$ has many characteristics, which are suitable for high voltage and high reliability capacitor applications. It also has high dielectric constant, high breakdown strength, and low leakage current density. It also has a large optical gap of 5.6 eV (Vali, 2007)

Cavalcante et al. (2007) studied the synthesis, characterizations, and optical absorption behavior of $SrZrO_3$ powders obtained by a chemical method. The results showed that the $SrZrO_3$ powders free of secondary phases and with orthorhombic

structure were obtained from the polymeric precursor method. Rietveld analysis confirmed the orthorhombic phase with space group *Pbmn*. Less variations in the lattice parameters were observed in crystalline $SrZrO_3$ powders heat-treated at 1,123 and 1,223 K for 2 h. XRD patterns suggested that the crystallization of $SrZrO_3$ powders started at 848 K while Raman analysis revealed that the $SrZrO_3$ powders treated at 748 K presented a beginning of structural order at short range. UV-visible spectra showed the presence of localized levels in the band gap of disordered $SrZrO_3$ powders, and these levels were reduced with the increase of structural order, as shown in Table 2.8.

Table 2.8 Data obtained of UV-visible spectra for $SrZrO_3$ obtained by different methods reported in literature

Method	Temperature (K)	Time	Optical gap (eV)
PPM	748	2 h	4.49
PPM	773	2 h	4.91
PPM	973	2 h	4.96
PPM	1,123	2 h	5.02
PPM	1,223	2 h	5.04
PPM	1,423	2 h	5.11
PPM	1,523	2 h	5.22
FZ	-	-	5.41
SGC	973	1 h	5.20
PLD	673	5 min	5.70
SG	773	5 min	4.63
MOD	873	-	5.50

PPM = polymeric precursor method; FZ = floating zone; SGC = sol-gel combustion; PLD = pulsed laser deposition; SG = sol-gel, and MOD = metallo-organic decomposition

Wong *et al.* (2001) studied the crystal structures and phase transitions in the $SrTi_xZr_{1-x}O_3$ solid solution. The results showed that superlattice reflections in the neutron diffraction patterns were proved to be the most reliable indicators of lower symmetry structures. At room temperature, the structures were orthorhombic *Pbnm* in the range of 0

$\leq x \leq 0.4$, tetragonal $I4/mcm$ in the range $0.4 \leq x \leq 0.95$, and cubic $Pm3m$ for $0.95 \leq x \leq 1$. Additionally, they studied the two room-temperature tetragonal samples ($x = 0.5$, 0.75) by using neutron diffraction methods for additional high variable temperature. The tetragonal-to-cubic phase transition for $SrTi_{0.5}Zr_{0.5}O_3$ occurred between 948 and 998 K, whereas that for $SrTi_{0.75}Zr_{0.25}O_3$ ocurred between 573 and 623 K.

2.12 Photocatalytic Degradation

2.12.1 Photocatalytic Oxidation

It is well established that conduction band electrons (e^-) and valence band holes (h^+) are generated when aqueous photocatalyst suspension is irradiated with light energy greater than its band gap energy. The photogenerated electrons can reduce the dye or react with electron acceptors, such as O_2 adsorbed on the photocatalyst surface or dissolved in water, reducing it to superoxide radical anion $O_2^{\cdot-}$. The photogenerated holes can oxidize the organic molecule to form R^+ or react with OH^- or H_2O, oxidizing them into $OH^\cdot$ radicals. Together with other highly oxidant species (peroxide radicals), they are reported to be responsible for the heterogeneous photocatalytic degradation of organic substrates as dyes. According to this, the relevant reactions at the semiconductor surface causing the degradation of dyes can be expressed as follows:

$$photocatalyst + hv(UV) \rightarrow photocatalyst(e_{CB}^- + h_{VB}^+) \qquad (1)$$

$$photocatalyst(h_{VB}^+) + H_2O \rightarrow photocatalyst + H^+ + OH^\cdot \qquad (2)$$

$$photocatalyst(h_{VB}^+) + OH^- \rightarrow photocatalyst + OH^\cdot \qquad (3)$$

$$photocatalyst(e_{CB}^-) + O_2 \rightarrow photocatalyst + O_2^{\cdot-} \qquad (4)$$

$$O_2^{\cdot-} + H^+ \rightarrow HO_2^\cdot \qquad (5)$$

$$Dye + OH^\cdot, HO_2^\cdot, O_2^{\cdot-} \rightarrow degradation\ products \qquad (6)$$

$$Dye + h_{VB}^+ \rightarrow oxidation\ products \qquad (7)$$

$$Dye + e_{CB}^- \rightarrow reduction\ products \qquad (8)$$

The resulting $OH^\bullet$ radical, being a very strong oxidizing agent (standard redox potential of +2.8 V), as well as $HO_2^\bullet$ and $O_2^{\bullet-}$, can oxidize most of azo dyes to the mineral end products. Substrates not reactive toward hydroxyl radicals are degraded employing photocatalysis with rates of decay highly influenced by the semiconductor valence band edge position. The role of reductive pathways (Equation (8)) in heterogeneous photocatalysis has been envisaged also in the degradation of several dyes but in a minor extent than oxidation.